Journal of Materials Chemistry A

Accepted Manuscript

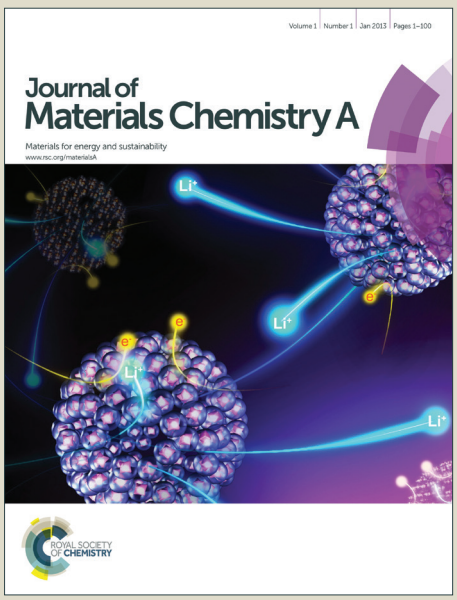

ROYAL SOCIETY OF CHEMISTRY

www.rsc.org/materialsA

Superior supercapacitive performance in electrospun copper oxide nanowire electrodes

Baiju Vidhyadharan,[1] Izan Izwan Misnon,[1] Radhiyah Abd Aziz,[1] K. P. Padmasree,[2] Mashitah M. Yusoff,[1] Rajan Jose[1]*

[1]Nanostructured Renewable Energy Materials Laboratory, Faculty of Industrial Sciences & Technology; [2]CINVESTAV, Unidad Saltillo, Carr. Saltillo - Monterrey km 13.5, C.P. 25900, Mexico; *E-mail: rjose@ump.edu.my

Abstract

Copper Oxide (CuO) nanowires of diameter ~30 – 50 nm are developed by an aqueous polymeric solution based electrospinning process and studied their structural, morphological, and electrochemical properties with an aim to fabricate high performance supercapacitor devices. The wires consist of densely packed cuboidal particles of size ~10 nm characterized by a low degree of crystal defects. Supercapacitor electrodes are fabricated on nickel foam substrates using 75 wt.% CuO in 15 wt.% conducting carbon and 10 wt.% polyvinylidene fluoride. The supercapacitive properties of the electrodes are evaluated in three-electrode configuration in aqueous electrolytes, viz. KOH and LiOH, employing cyclic voltammetry (CV), charge – discharge cycling (CDC) and electrochemical impedance spectroscopy (EIS). A record specific capacitance (C_S) is observed for the present electrospun CuO nanowires: C_S ~620 Fg^{-1} in KOH and 581 Fg^{-1}in LiOH at a current density of 2 Ag^{-1} with Coulombic efficiency ~100%. Compared with the previous results on the electrochemical stability of CuO nanostructures, the material electrospun using aqueous polymeric solution showed much higher operational stability (98% at the end of 1000 cycles and 92% at the end of 2000 cycles) owing to their superior crystallinity. Electrochemical properties of the electrodes were determined using EIS to validate the CV and CDC results.

Keywords: Electrochemical energy storage, hybrid capacitors, renewable energy, metal oxide semiconductors, , batteries, one dimensional nanostructures.

1. Introduction

A fast-growing market of portable electronic devices and hybrid electric vehicles (HEVs) have lead intense research in the area of electrical energy storage devices characterized by high energy density (~100 – 200 $Whkg^{-1}$), power density (≥5 $kWkg^{-1}$) and long cycle life (≥10^5 cycles). Supercapacitors represent a unique class of energy storage devices including electric double layer capacitors, pseudocapacitors, and hybrid capacitors; recent review articles on this topic may be found elsewhere.[1–6] Electric double layer capacitors (EDLC) store electrical energy via accumulation of electric charges at an electrical double layer formed at the interface between a mesoporous electrode and an electrolyte. Carbon structures such as activated carbon, carbon nanotubes, and graphene are choices to build EDLCs. No electron transfer takes place across the electrode interface during its operation; and therefore, this charge storage process is non-faradic[7]. The pseudocapacitors involve faradic charge storage process facilitated by a redox reaction at the electrode – electrolyte interface.[8,9] Transition metal oxides (TMOs) and conducting polymers show high pseudocapacitance; a theoretical pseudocapacitance equal to $F / (\Delta E \times m)$, where F is the Faraday constant, m is the molecular weight and ΔE is the redox potential of the material, could be achieved by TMOs.[10] A high specific surface area of the electrode material to enable a large electrode – electrolyte interface for efficient redox reaction, high electrical conductivity to enable high rate charging and discharging, and faster ion diffusivity are properties of TMOs and electrolytes required to achieve higher energy and power densities in pseudocapacitors.

The copper oxide (CuO) is typically interesting among the TMO nanostructures because of relatively lower toxicity, larger abundance and lower cost thereby, environmental stability, and desirable optical, electrical and electrochemical properties. The CuO showed promising specific capacity and charge-discharge cycling when used as an electrode material for rechargeable Li-ion battery.[11] For its application in pseudocapacitors, theoretically CuO could deliver a pseudocapacitance (C_P)~1800 Fg^{-1} (See Supplementary Information S1), a value closer to that of widely studied hydrated ruthenium oxide ($RuO_2.nH_2O$) (~2200 Fg^{-1}). Therefore, many research groups are considering CuO as a supercapacitor electrode recently, a brief summary of which is in Table 1.[12–17] In their efforts, CuO nanostructures of diverse morphologies such as nanoflakes,[12] flower-like structures,[13,17]nanowires,[14] nanosheets,[15] and nanoflowers.[14,16] are tested. However, the specific capacitance (C_S) attained in most of these morphologies is ≤ 15% of its theoretical value with an exception of nanosheets grown by template method that showed up to ~32% [15](Table1).

One of the preliminary requirements for a material to be selected as an electrode for a high performance pseudocapacitors device, apart from a redox reaction, is high electrical conductivity; and therefore, one-dimensional morphologies are attractive owing to their directional charge transport properties. Among the many nanowire forming techniques, electrospinning represents a simple and versatile technique for producing nanostructured advanced materials as well as membranes for many engineering applications to be enabled such as filtration, healthcare, and energy. [18–20] In the electrospinning technique, a polymeric solution, usually prepared in organic solvents, is injected through a syringe needle in the presence of an electric field. A polymeric jet is initiated upon injection of the solution that undergoes asymmetric bending during the passage between the injector and the collector. This asymmetric bending increases the path length of the jet and allows the solvent to evaporate thereby producing solid continuous fibers with diameters ranging from nanometers

to sub-micrometers on a collector surface. If the polymeric solution contains precursors for forming an inorganic solid, then appropriate annealing produces its continuous nanofibers.[21] However, evaporation of large volume of organic solvents during electrospinning have adverse environmental effects; this drawback is removed in "greener" electrospinning using aqueous polymeric solutions.

This paper deals with electrospinning of CuO nanowires using an aqueous polymeric solution with ultra-low diameter (<50 nm) and evaluation of their electrochemical properties for fabrication of a supercapacitor device. The electrode showed C_S up to ~35% of the theoretical value and showed excellent electrochemical cycling in popular aqueous electrolytes, viz. KOH and LiOH. Our results demonstrate that the present electrospun CuO nanowires could be a choice of supercapacitor electrode material characterized by high C_S and related properties.

2. Experimental Details

2.1 Synthesis and characterization of CuO nanowires

A previously reported procedure with modification was chosen for electrospinning of CuO nanowires.[22] Starting materials were copper acetate monohydrate [$Cu(CH_3COO)_2.H_2O$; CuAc; 99%; R&M Chemicals] and polyvinyl alcohol (PVA; Mw– 145000, Merck). In a typical synthesis, CuAc (1 g) was dissolved in 20 mL aqueous PVA solution (7 wt.% PVA in water) thereby forming a 0.63 M stock solution, which was stirred for 20 h at room temperature. The as-prepared solution was electrospun using a commercial electrospinning unit (Electroris, nanoLab, Malaysia) at 0.5 mlh^{-1} and at ~24 kV. The solid fibres were collected at a distance ~17 cm away from the spinneret. The relative humidity of the electrospinning chamber was maintained at ~30%. The as-spun fibers were calcined at 500 ^oC for 1 h in air.

Crystal structure of the material was studied by X-ray diffraction (XRD) technique using Rigaku Miniflex II X-ray diffractometer employing Cu Kα radiation (λ = 1.5406 Å). Morphology and microstructure of the materials were studied by scanning electron microscopic technique (7800F, FESEM, JEOL, USA). High resolution lattice images and selected area diffraction patterns were obtained using transmission electron microscope (TEM) operating at 300 kV (FEI, Titan 80-300 kV). The BET surface area of the material was measured using gas adsorption studies employing a Micromeritics (Tristar 3000, USA) instrument in the nitrogen atmosphere.

2.2. Preparation of electrodes for cyclic voltammetry

Supercapacitor electrodes were fabricated on pre-cleaned nickel foam substrates. The nickel foam was cleaned by degreasing in acetone, etching in 1M HCl for 15 minutes, and subsequently washing in water and ethanol for 5 min each. The working electrode was prepared by mixing the CuO nanowires with polyvinylidene fluoride (PVDF) (Sigma Aldrich) and carbon black (Super P conductive, Alfa Aesar) in the ratio 75:15:10. The above mixture was stirred in N-methyl-2-pyrrolidinone for better homogeneity. The as-prepared slurry was then pasted on a nickel foam substrate (area ~1 cm^2) and dried in an oven at 60 °C for 24 h. The mass-loading of the active material was ~2.5 mg/cm^2. The dried electrode was then pressed using a pelletizer at a pressure of 5 ton. Electrochemical properties of the devices were studied by cyclic voltammetry (CV), galvanoststic charge–discharge cycling (CDC), and electrochemical impedance spectroscopy (EIS) in KOH and LiOH electrolytes. The electrochemical properties in three-electrode configuration were obtained at room temperature using a potentiostat-galvanostat (PGSTAT M101, Metrohm Autolab B.V., The Netherlands) employing NOVA 1.9 software. A platinum rod and a saturated Ag/AgCl electrode were used as the counter and the reference electrodes, respectively.

3. Result and Discussion

3.1 Synthesis and Characterization of CuO nanowires

Figure 1 shows the FESEM images of the as-prepared and annealed nanowires. The as-prepared wires were uniform and had an average diameter of ~210 nm, which upon annealing reduced to ~30 – 50 nm. i.e., the wires showed a lowering of over 300% in diameter upon annealing. The diameter of these wires are 50 – 60% lower than that obtained through the previous reports (100 – 200 nm),[23,22] which resulted from the high molecular weight of the polymer used in our work.[24] Lower diameter of the wires was further confirmed by TEM measurements (Figure 2). The bright field image in Figure 2(a) shows that the wires are formed of particles of size ~10 – 20 nm. The particles were of well faceted cuboidal morphology with sharp edges (See Supplementary Information S2a). A selected area diffraction pattern (SAED) of a typical nanowire segment is in the inset of Figure 2(a). The SAED pattern consists of diffraction spots oriented in typical polycrystalline ring patterns which further confirm the high degree of particle orientation in the nanowires. Figure 2(b) shows a high resolution lattice image of a typical particle; well ordered lattice fringes are clearly visible in the TEM images (more figures in Supporting Information S2b). The particles are free from crystal defects such as line and point defects; therefore, they are called as "highly crystalline".

The measured BET surface area of the CuO nanowires was ~14 m^2/g with a pore volume of ~0.5 cm^3/g, which are at lower end for wires of diameter ~30 – 50 nm. The observed relatively lower surface area is partly contributed by dense particle packing in the wires that reduced porosity despite the lower wire diameter. The Barrett-Joyner-Halenda (BJH) analysis showed a mean pore size of ~11.5 nm because the dense particle packing resulted in larger pores (See the TEM images in the Supporting Information S2a).

Fig. 3 shows the XRD pattern of the annealed CuO and refined using the PowderCell 2.3 program[25]. All the peaks fit well to a monoclinic unit cell (Space group $C12/c_1$, #15) with lattice parameters a = 4.598 Å, b = 3.46 Å, c= 5.135 Å and β = 99.30°, which correspond to reported values (PDF Card No: 45-0937). The XRD peaks showed line broadening on account of the lowering of particle size; the crystallite size calculated using the Scherrer formula was ~20 nm, which is in good agreement with the particle size determined from the HRTEM micrographs. All these studies confirm that the materials produced through the present approach is single phase nanowires of CuO.

3.2 Electrochemical properties of CuO nanowires

3.2.1. Cyclic Voltammetry

Figure 4 summarizes the results of CV studies. The CV curves recorded in varying electrolyte concentrations showed that the devices work well for 6M KOH (Figure 4a), consistent with the previous results on CuO nanosheet arrays that showed the highest C_S,[15] and 3M LiOH (See Supplementary Information S3). A small increase in charge polarization but accompanied by a lowering of voltammetric current was observed in the 8M KOH compared to the 6M analogue which is expected to arise from the difference in their ionic conductivities (σ_i). The σ_i is 626.6 mS/cm for 6M KOH and 597.6 S/cm for 8M KOH at constant potential.[26] Figures 4 (b) & (d) are the CV curves of the CuO nanowires in the 3M KOH & LiOH electrolytes, which shows oxidation (anodic) and reduction (cathodic) events indicative of the pseudocapacitance charge storage mechanism. However, shape of the CV curves are considerably different in the two electrolytes arising from the difference in the charge stored during the redox reaction.[27]The CV of the nanowires in 6M KOH is in Figure 4(c) to compare our results with best performing devices in the literature (Table1). The ratio between the amount of charge involved in the reduction and the oxidation events, which is obtained from the respective integrated area under the CV curve, is a measure of Coulombic

efficiency (η) of the system. The η of the present electrospun CuO nanowires is calculated to be 98, 96, and 100% in 3M KOH, 6M KOH, and 3M LiOH electrolytes, respectively.

The electrochemical behaviour of CuO nanostructures in alkaline electrolyte is studied extensively.[28–34] The oxidation and reduction events in CuO in aqueous electrolytes such as KOH and LiOH occur in the potential range 0–0.6 V.[32] During charging, the electrode material, i.e., CuO, undergo a reduction process and give rise to cathodic peaks in the CV curve. The cathodic peaks in the Figure 4, i.e., C_1&C_2 (inset of the panels b,c, and d) are attributed to reduction of CuO/$Cu(OH)_2$ to Cu_2O/CuOH.[28,31–33] Figures in the inset is given in the Supplementary Information S4 for better clarity. These assignments are based on the X-ray photoelectron spectroscopy and XRD measurements of alkali treated CuO by Nakayama et al.[34] as well as by correlating the force curves in atomic force microscopy and CV data by Kang et al[32]. Electrochemical events during the discharge cycle is displayed in the CV curves by the anodic peaks A_1 &A_2 (Figure 4), which are attributed to the oxidation of Cu_2O/CuOH to CuO/$Cu(OH)_2$.[28,31–33] The oxidized species are also verified by Kang et al.[32] Further studies show that reduction of CuO/$Cu(OH)_2$ to Cu and the oxidation of CuO/$Cu(OH)_2$ to Cu (III) species do not occur in the 0 – 0.6 V potential range.[33,34]Therefore, based on the present CV data and previously reported experimental results, the charging and discharging processes in the CuO electrode in the potential range 0 – 0.6 V could be summarized in the following reactions. [28–34]

$$2CuO + H_2O + 2e^- \underset{Discharging}{\overset{Charging}{\rightleftharpoons}} Cu_2O + 2OH^-$$

$$Cu(OH)_2 + e^- \underset{Discharging}{\overset{Charging}{\rightleftharpoons}} CuOH + OH^-$$

The CV curves marked lower slopes for lower scan rates, which indicate that lower scan rates allow longer duration for the anions to access the bulk of the electrode; thereby showing ideal

capacitive behavior. However, with increase of the scan rate the anodic peak shifts towards positive potentials and the cathodic peak shifts towards the negative potentials as was observed conventionally.[35] The C_S is normally decreased with increasing scan rates due to the above reasons.

The C_S (Fg^{-1}) of the samples was estimated from the cathodic or anodic part of the CV data using the equation:

$$C_S = \frac{1}{mv(E_2 - E_1)} \int_{E_1}^{E_2} i(E)dE \qquad (1)$$

where E_1 and E_2 are the cutoff potentials in the CV curves and $i(E)$ is the current at each potential, $E_2 - E_1$ is the potential window, m is the mass of the active material, and v is the scan rate. Figure 4(e) compares the C_S of the CuO nanowires at scan rates in the 2 – 70 mV/s range in the voltage window 0 – 0.6 V for the two electrolytes. The 3M KOH showed a C_S of ~404 Fg^{-1} at 2 mVs^{-1} scan rate which in the case of LiOH was 45% larger as predicted by the difference in their CV behaviour (Figure 4 b&d). However, a C_S of ~710 Fg^{-1} was recorded in 6M KOH, which is the highest value reported for any CuO structures (Table 1). The C_S remained practically same for higher scan rates (>30 mVs^{-1}) primarily because the ion movement is limited only to the surfaces of the electrode material at such conditions. The EDLC is the dominant mechanism at higher scan rates. Majority of active surface are utilized by the ions for charge storage at the lower scan rates (< 5 mV/s), thereby resulting in the higher C_S.

In pseudocapacitive materials, such as CuO, the scan rate (v) dependence of voltammetric current (i) is analyzed to determine whether the capacitance originates from surface redox reaction or from bulk diffusion. The $i \propto v$ for surface redox reaction and $i \propto \sqrt{v}$ for semi-infinite bulk diffusion.[2] Figure 5 shows the peak current as a function of v and $\sqrt{v}$ for the electrolytes used here. In the case of 3M KOH, the peak current varied

linearly with scan rate (Figure 5a) whereas it varied with square root of scan rate for 3M LiOH and 6M KOH (Figure 5b). Therefore, the capacitance originated from surface redox reaction in the case of 3M KOH whereas for the other two electrolytes bulk diffusion occurred.

Figure 5 explains very well the drastic variation in the C_S as a function of scan rate observed in Fig. 4(e). The C_S showed a drastic variation with scan rate in the 3M LiOH and 6M KOH whereas it was practically same for the 3M KOH electrolyte. Generally, the ion movement is limited only to the surfaces of the electrode material at higher voltammetric scan rates (>30 mVs^{-1}). Therefore, the contribution from the bulk diffusion is no longer available in the case of 3M LiOH and 6M KOH electrolytes and the C_S drop off drastically. On the other hand, the C_S originated from the surface redox reaction in 3M KOH and remained practically constant with scan rate.

3.3.2. Galvanostatic charge – discharge studies

The supercapacitive performances of the CuO nanowire electrodes were evaluated from the galvanostatic CDC curves. The maximum attainable potential is ~0.4 V in the KOH and ~0.6 V in the LiOH electrolytes. Figure 6 shows the CDC curves in the potential window ~0–0.4 V in the KOH electrolyte and ~0 – 0.6 V in the LiOH electrolyte. Our experiments show that the operating potential window of the CuO electrodes could be extended using appropriate choice of electrolytes. The CuO electrodes showed a potential of ~1 V in aqueous 1M Na_2SO_4 electrolyte (See Supplementary Information S5). Furthermore, Zhang et al reported an operating potential as high as 2.5 V in supercapacitor electrodes containing a mixture of CuO nanobelts and single walled carbon nanotubes (SWCNT) in $LiPF_6$ electrolyte with appreciable energy and power densities.[36] Nevertheless, a working supercapacitor in an asymmetric device configuration further enhances the operating potential taking advantages of the high voltage window of the carbon electrodes (cathode) and high

capacitance of the pseudocapacitor electrode (anode).[27] Therefore, although the potential window of the present CuO electrodes is comparatively lower many remedies including varied choice of electrolytes and fabrication of composites with carbon structures are reported to tune the operating voltage of a supercapacitor device for practical applications.

Figures 6 (a,b & c) show the first three charge discharge curves of the CuO nanowire electrode at a galvanostatic current density 2 Ag^{-1} (5 $mAcm^{-2}$) in 3 & 6M KOH and in 3M LiOH electrolytes, respectively. The potential drop between the charge and discharge curves is generally caused by the internal resistance and incomplete faradic reaction in the electrode. The internal resistance, which was calculated from the ratio of initial potential drop (V_{IR}) to the corresponding discharge current (I_D), of the electrode was ~8 mV in the KOH and ~14 mV in the LiOH electrolytes. The lower internal resistance could be attributed to the high electrical conductivity offered by less-defective particles forming the electrospun nanowires (Figure 2b and Supplementary Information S2b).[37] Relatively high ionic conductivity of the KOH electrolyte compared to that of LiOH[27,26] further reduced the potential drop in corresponding electrodes.

Figure 6 (a_1, b_1 & c_1) shows the galvanostatic discharge behavior of the electrodes in the two electrolytes as a function of current density from where the practically available C_S could be calculated. The discharge behaviour was visibly different in 6M KOH compared to the other two. The devices using the 6M KOH electrolytes showed three segments, viz. (i) a fast initial potential drop followed by (ii) a slow potential decay, and (iii) a faster potential drop corresponding to the EDLC. The first two sections are assigned to the reduction of $CuO/Cu(OH)_2$ to $Cu_2O/Cu(OH)$ as observed from the CVs. However, the fast decay of the first segment is not observed for the devices with 3M KOH & LiOH electrolytes due to their inferior ionic conductivity.

The C_S was calculated from the discharge curve using the relation

$$C_S = \frac{It}{m\Delta V} \qquad (2)$$

where I, t, m and ΔV are applied current, discharge time, active mass, and open potential, respectively. The charge/discharge curves in Figure 6 (a_1, a_2 & a_3) indicate that most of the capacitance is generated in the potential range of 0.23 to 0.4 V in KOH and 0.32 to 0.6 V in 3M LiOH, corresponding to the redox between Cu(I) and Cu(II).

Figure 7 shows the variation of C_S as a function of specific current density for the two electrolytes. Note that contribution of C_S from the substrate was studied in the two electrolytes and appropriate corrections were applied in the generation of Figure 7(See Supplementary Information S6 & S7). The C_S decreased with increasing specific current density similar to that observed in the CV measurements. The total C_S has contribution from both C_p and EDLC. The C_S of the CuO nanowire electrode evaluated from the discharge curve is ~620 Fg^{-1} (6M KOH) and 581 Fg^{-1} (3M LiOH) at a current density of $2Ag^{-1}$.

The C_S reported herewith is currently the highest value reported for the CuO electrodes (Table 1). The larger C_S of CuO nanowires could be attributed to (i) the lower wire diameter that enhances the available surface area; (ii) high electrical conductivity owing to the one-dimensional morphology; (iii) and superior crystallinity. Lower diameter (≤ 50 nm) of the nanowires also reduces the electrolyte diffusion distance thereby maximizes the active surface area for adsorption and desorption of OH^- ions and enhances the C_S.[31–33,38] It is worth noting that C_S achieved using a composite electrode containing CuO and SWCNT[36] is only ~20% of that has been achieved by the present CuO nanowires. Performance of an asymmetric capacitor employing CuO as one of the electrodes is not reported herewith; purpose of the present paper is a thorough understanding on the electrochemical properties of the electrospun CuO nanowires developed from an aqueous polymeric solution.

Effects of the high crystallinity of the present electrospun CuO nanowires are more evident in the cycling stability of the devices fabricated in this study. Figure 8 summarizes the stability of electrochemical cycling of the CuO nanowires. The device showed good cycling behaviour with ~99% C_S retention in 3M KOH & LiOH and 98% in 6M KOH at the end of 1000 cycles (Figure 8a). However, a more pronounced loss in C_S was observed in the 1001 – 2000 range of cycles (See Supplementary Information S8). A capacity fading of ~5% was observed in this range for the 3M KOH & LiOH and ~8% for the 6M KOH electrolytes. The device was physically stable; the active material stuck well with nickel foam substrate even at the end of 2000 cycles.

Nevertheless, capacity fading in the present CuO nanowires is lower than that is reported for most CuO nanostructures (Table 1). To be specific, compared to the ~18% capacity fading in just 500 cycles in the electrode reported the highest C_S until this work, i.e., in the CuO nanosheets synthesized using the template growth method,[14] the capacity fading of ~10% in the present work with superior C_S for 2000 cycles is certainly advantageous.

The Columbic efficiency (η) of the devices was calculated from its charging (T_c) and the discharging (T_d) times from CDC curves following the relation,

$$\eta = \frac{T_d}{T_C} \times 100 \qquad (3).$$

Initial η of the device was ~100%, which remained practically same in the 3M KOH & LiOH electrolytes but reduced to ~99% in the 6M KOH at the end of 1000 cycles (Figure 8b). In the 1001 – 2000 range of cycles, a small lowering (1%) in the η was observed in the 3M KOH; however, it further lowered to 92 and 90% in the 3M LiOH and 6M KOH electrolytes, respectively (See Supporting Information S8). Reason for this variation is investigated and found that the internal resistance of the devices steadily increased in the 1000 – 2000 intervals in 6M KOH and 3M LiOH whereas it was nearly a constant for 3M KOH (See

Supporting Information S8). Gradual increase in the internal resistance could be attributed to incomplete reversal of the faradic process during the discharge process.[39,40]

The C_S retention and η are at the upper limit reported for CuO nanostructures (Table 1), which are most likely resulted from the dense packing and larger pore diameter of the present electrospun CuO nanowires. The relationship between surface area, pore size, and C_S is well documented in literature.[41] All pores in a nanocrystalline material, although they increase the surface area, do not contribute to the C_S.[41] Those pores with diameter larger than the size of the solvated electrolyte ion only contribute to the C_S. Size of the hydrated OH^- ion in the KOH and LiOH electrolyte is 0.113 nm, which is an order of magnitude lower than the pore size in the present CuO nanowire (11.5 nm). These larger pores provide clear adsorption/desorption pathways thereby increasing the cycling stability.

3.3.3 Electrochemical Impedence Spectroscopy studies

Electrochemical impedance spectroscopy (EIS) measurements were carried out to determine the charge kinetics of the device associated with the above described supercapacitive parameters. Figure 9 shows the Nyquist plot of the CuO nanowire electrode determined by EIS in the frequency range 10 kHz – 0.01 Hz at open circuit potential both in the 6M KOH and the 3M LiOH. The EIS spectra of a supercapacitor electrode are usually deconvoluted to three segments following three processes; (i) the equivalent series resistance (ESR) of the device at high frequency (> 1 kHz); (ii) Warburg diffusion region resulting from the frequency dependence of ion diffusion/ transport in the electrolyte at the intermediate frequencies (500 – 5 Hz); and (iii) capacitive effects at low frequencies (<5 Hz).[42,43] The high frequency off-set of the EIS spectrum is a combination of (i) electrolyte resistance (ii) intrinsic resistance of the electro active material, and (iii) the contact resistance between the active material and the current collector, which is a measure of ESR. The ESR of the present CuO nanowires is determined to be 0.67 Ω in 3M KOH, 0.56 Ω in 6M KOH and 0.72 Ω in

3M LiOH; this relatively lower ESR could be attributed to the one dimensional morphology and superior crystallinity of the CuO nanowires.[44] The EIS spectra displayed a small semicircle at the high frequency region, representing the redox reaction between Cu(I) and Cu(II), followed by a linear portion extending in the middle and low frequency regions. The diameter of the semicircle represents the kinetic resistance to the ion transfer, known as charge transfer resistance (R_{ct}) of the redox reactions. The R_{ct} is rather low for the present CuO nanowires; 0.39 Ω in 3M KOH, 0.32 Ω in 6M KOH and 0.45 Ω in 3M LiOH which is attributed to improved ionic conduction and electrolyte diffusion through the pores of the electrode material.[45]

The low frequency region (<1 Hz) of the second segment of the EIS curve indicates the electrically charged electrode – electrolyte interface that generates the supercapacitive behavior of the device. Total charges accumulated at the electrode – electrolyte interface represent the maximum achievable capacitance by the system. The linearity of this portion of EIS also reveals that the ionic penetration and accumulation of charges at the available electrode surface are time-dependent processes. The characteristics of a supercapacitor, viz. the energy (E_S) and power densities (P_S), could be evaluated from this segment of the EIS by expressing the total capacitance as a combination of real (C') and imaginary parts (C'') [46,47]

$$C(\omega) = C'(\omega) + C''(\omega) \qquad (3),$$

where $C'(\omega) = -Z''(\omega) \Big/ \omega|Z(\omega)|^2$ and $C''(\omega) = Z'(\omega) \Big/ \omega|Z(\omega)|^2$.

The C' is a measure of charge stored as a function frequency, representing the E_S and C'' corresponds to the energy dissipation occur during charge storage. Figure 10 (a & b) show the variation of C' and C'' as a function of frequency. The C' asymptotically decreases as frequency increases. The C' of the CuO nanowires in the KOH electrolyte is higher than that in the LiOH electrolyte consistent with the CDC results. However, the C' determined from

the EIS does not coincide with that determined from other measurements; this discrepancy is attributed to factors such as physical and chemical heterogeneities and deeply trapped ions that remain immobile during EIS measurements.[48,49]

The *C"* showed a bell-shaped curve (Figure 10), the frequency corresponding to the peak (f_o) represents the point where the device changes from purely resistive to purely capacitive circuit[50] and is a measure of charge relaxation time (τ) defined by $\tau = 1/f_o$.[46] The τ quantitatively measures how fast a supercapacitor is discharged (i.e., power density). Behaviour of the electrodes in the two electrolytes is noticeably different, the f_o determined from the graph are at 31 mHz in 3M LiOH, 30.8 mHz, and 3.7 Hz in 3M & 6M KOH, respectively. The τ is calculated to be 32.3s, 0.270 s, 32.4s in 3M LiOH, 6M KOH and 3M KOH, respectively. i.e., power capability of CuO nanowire electrode in 6M KOH is higher than that in 3M LiOH consistent with the observations from CDC measurements.

Finally, the specific energy (E_S) and power densities (P_S) of the CuO electrode were calculated from the CDC measurements employing the relations[51]

$$\left.\begin{aligned} E_S &= \frac{1}{2} C_S V^2; \\ P_S &= \frac{E}{\Delta t} \end{aligned}\right\} \qquad (4)$$

where Δt is the discharge time. Figure 11 is the Ragone plot showing the E_S *vs*. P_S of the CuO electrode. Commendable variation in E_S of the electrode was observed between the three electrolytes; the 3M LiOH showed highest E_S compared to the KOH analogues on account of the higher potential window achievable in the former (0.6 V). No drastic variation in E_S was observed with P_S for all the electrolytes used here. The CuO electrode in 3M LiOH delivered E_S of 16.4, 18.6, 20.6, 23.1, 29 Whkg^{-1} at P_S of 3.28, 2.65, 1.9, 1.24, 0.65 kWkg^{-1}, respectively. Although EIS showed lower τ , that predicts larger P_S, for the 6M KOH

electrolyte the observed high value in the LiOH electrolyte results from the high E_S achieved through the larger potential window.

4. Conclusion

In conclusion, we have shown that CuO wires of diameter ~30 – 50 nm with excellent crystallinity could be synthesized by employing an aqueous polymeric solution based electrospinning protocol . These nanowires are shown to be characterized by desirable electrochemical properties for fabrication of a high performance supercapacitor device. A supercapacitor electrode fabricated using the CuO nanowires showed a record specific capacitance, accounting ~35% of its theoretical capacitance, consistently from cyclic voltammetry and galvanostatic charge – discharge cycling experiments. The CuO nanowires synthesized by electrospinning an aqueous polymeric solution is currently the record holder in terms of specific capacitance and electrochemical stability among diverse CuO morphologies tested as a supercapacitor electrode. Electrochemical impedance spectroscopy and galvanostatic cycling showed that the equivalent series resistance and internal resistance of the devices are rather low on account of the one-dimensionality of the electrode material. Our results demonstrate that the present electrospun CuO could be an acceptable choice to build high performance energy storage devices.

Acknowledgements

This work was supported by Ministry of Higher Education (MOHE), Malaysia under Exploratory Research Grant Scheme (RDU110103) and Fundamental Research Grant Scheme (RDU 110602) on energy storage devices; and Malaysian Technological Universities Network (MTUN) grant on nanowires of metal oxide semiconductors. Research and Innovation Department, UMP is acknowledged for internal support.

Supporting Information available:

Calculation of specific capacitance (S1); Bright field transmission electron micrographs (S2a) and high resolution lattice images (S2b), cyclic voltammograms of the CuO nanowires electrodes at varying concentrations of LiOH solution at a scan rate of 10 mVs^{-1} for optimising the electrolyte concentration for charge –discharge cycling (S4); charge – discharge cycling in 1M Na_2SO_4 (S5); discharging curves of the Ni foam substrate in 6M KOH to compare the discharge times with and without CuO nanowires (S6, S7); Cycling stability, Coulombic efficiency, and internal resistance of the electrodes during 1001 – 2000 cycles calculated from the CDC curves (S8). These documents are freely available from the internet via: http://www.rsc.org

References:

1. Q. Lu, J. G. Chen, and J. Q. Xiao, *Angew. Chem. Int. Ed. Engl.*, 2013, **52**, 1882–9.
2. I. E. Rauda, V. Augustyn, B. Dunn, and S. H. Tolbert, *Acc. Chem. Res.*, 2013, **46**, 1113–1124.
3. A. K. Shukla and T. Prem Kumar, *Wiley Interdiscip. Rev. Energy Environ.*, 2013, **2**, 14–30.
4. S. Park, M. Vosguerichian, and Z. Bao, *Nanoscale*, 2013,**5**, 1727–1752.
5. S. Chen, W. Xing, J. Duan, X. Hu, and S. Z. Qiao, *J. Mater. Chem. A*, 2013, **1**, 2941.
6. J. Jiang, Y. Li, J. Liu, X. Huang, C. Yuan, and X. W. Lou, *Adv. Mater.*, 2012, **24**, 5166–5180.
7. Y. Bin Tan and J.-M. Lee, *J. Mater. Chem. A*, 2013, **1**, 14814–14843.
8. L. L. Zhang and X. S. Zhao, *Chem. Soc. Rev.*, 2009, **38**, 2520–2531.
9. B. E. Conway, *J. Electrochem. Soc.*, 1991, **138**, 1539–1548.
10. H. Li, J. Wang, Q. Chu, Z. Wang, F. Zhang, and S. Wang, *J. Power Sources*, 2009, **190**, 578–586.
11. L. B. Chen, N. Lu, C. M. Xu, H. C. Yu, and T. H. Wang, *Electrochim. Acta*, 2009, **54**, 4198–4201.
12. Z. Endut, M. Hamdi, and W. J. Basirun, *Thin Solid Films*, 2013, **528**, 213–216.
13. D. P. Dubal, G. S. Gund, C. D. Lokhande, and R. Holze, *Mater. Res. Bull.*, 2013, **48**, 923–928.
14. Y. Li, S. Chang, X. Liu, J. Huang, J. Yin, G. Wang, and D. Cao, *Electrochim. Acta*, 2012, **85**, 393–398.
15. G. Wang, J. Huang, S. Chen, Y. Gao, and D. Cao, *J. Power Sources*, 2011, **196**, 5756–5760.
16. H. Zhang, J. Feng, and M. Zhang, *Mater. Res. Bull.*, 2008, **43**, 3221–3226.
17. Y. Hsu, Y. Chen, and Y. Lin, *J. Electroanal. Chem.*, 2012, **673**, 43–47.
18. D. H. Reneker and A. L. Yarin, *Polymer*, 2008, **49**, 2387–2425.
19. W. Sigmund, J. Yuh, H. Park, V. Maneeratana, G. Pyrgiotakis, A. Daga, J. Taylor, and J. C. Nino, *J. Am. Ceram. Soc.*, 2006, **89**, 395–407.

20. S. Ramakrishna, R. Jose, P. S. Archana, A. S. Nair, R. Balamurugan, J. Venugopal, and W. E. Teo, *J. Mater. Sci.*, 2010, **45**, 6283–6312.

21. N. Bhardwaj and S. C. Kundu, *Biotechnol. Adv.*, 2010, **28**, 325–47.

22. H. Guan, C. Shao, B. Chen, J. Gong, and X. Yang, *Inorg. Chem. Commun.*, 2003, **6**, 1409–1411.

23. R. Sahay, J. Sundaramurthy, P. Suresh Kumar, V. Thavasi, S. G. Mhaisalkar, and S. Ramakrishna, *J. Solid State Chem.*, 2012, **186**, 261–267.

24. D. Li and Y. Xia, *Nano Lett.*, 2003, **3**, 555–560.

25. W. Kraus and G. Nolze, *J. Appl. Crystallogr.*, 1996, **29**, 301–303.

26. R. Gilliam, J. Graydon, D. Kirk, and S. Thorpe, *Int. J. Hydrogen Energy*, 2007, **32**, 359–364.

27. B.E. Conway, in "Electrochemical Supercapacitors" *Kluwer Academic/Plenum Publishers, NewYork*, 1997.

28. G. M. Brisard, J. D. Rudnicki, F. Mclarnon, and E. J. Cairns, *Electrochim. Acta*, 1995, **40**, 859–865.

29. L. D. Burke, M. J. G. Ahern, and T. G. Ryan, *J. Electrochem. Soc.*, 1990, **137**, 553–561.

30. J.-B. He, D.-Y. Lu, and G.-P. Jin, *Appl. Surf. Sci.*, 2006, **253**, 689–697.

31. M. Jayalakshmi and K. Balasubramanian, *Int. J. Electrochem. Sci*, 2008, **3**, 1277–1287.

32. M. Kang and A. Gewirth, *J. Phys. Chem. B*, 2002, **106**, 12211–12220.

33. S. M. A. E. Haleem and B. G. Ateya, *J. Electroanal. Chem.*, 1981, **117**, 309–319.

34. S. Nakayama, Atsushi Kimura, M. Shibata, S. Kuwabatia, and T. Osakai, *J. Electrochem. Soc.*, 2001, **148**, B467–B472.

35. Y. Li, B. Tan, and Y. Wu, *J. Am. Chem. Soc.*, 2006, **128**, 14258–9.

36. X. Zhang, W. Shi, J. Zhu, D. J. Kharistal, W. Zhao, B. S. Lalia, H. H. Hng, Q. Yan, *ACS Nano*, 2013, **3**, 2013–2019.

37. P. S. Archana, R. Jose, C. Vijila, and S. Ramakrishna, 2009,**113**, 21538–21542.

38. V. Maurice, H. Strehblow, and P. Marcus, 2000, **458**, 185–194.

39. L. Y. Chen, J. L. Kang, Y. Hou, P. Liu, T. Fujita, A. Hirata, and M. W. Chen, *J. Mater. Chem. A*, 2013, **1**, 9202.

40. S.Trasatti. and P. Kurzweil, *Platin. Met. Rev.*, 1994, **38**, 46.

41. C. Largeot, C. Portet, J. Chmiola, P. Taberna, Y. Gogotsi, and P. Simon, *J. Am. Chem. Soc.* 2008, **130**, 2730–2731.

42. P. Sen and A. De, *Electrochim. Acta*, 2010, **55**, 4677–4684.

43. J. H. Jang, S. Han, T. Hyeon, and S. M. Oh, *J. Power Sources*, 2003, **123**, 79–85.

44. X. Yan, J. Chen, J. Yang, Q. Xue, and P. Miele, *ACS Appl. Mater. Interfaces*, 2010, **2**, 2521–9.

45. F. Lisdat and D. Schäfer, *Anal. Bioanal. Chem.*, 2008, **391**, 1555–67.

46. C. Portet, P. L. Taberna, P. Simon, and E. Flahaut, *J. Power Sources*, 2005, **139**, 371–378.

47. C.-C. Hu and W.-C. Chen, *Electrochim. Acta*, 2004, **49**, 3469–3477.

48. D. Wang, W. Ni, H. Pang, Q. Lu, Z. Huang, and J. Zhao, *Electrochim. Acta*, 2010, **55**, 6830–6835.

49. A. S. Adekunle and K. I. Ozoemena, *Electroanalysis*, 2011, **23**, 971–979.

50. P. L. Taberna, P. Simon, and J. F. Fauvarque, *J. Electrochem. Soc.*, 2003, **150**, A292–300.

51. X. Zhang, D. Zhao, Y. Zhao, P. Tang, Y. Shen, C. Xu, H. Li, and Y. Xiao, *J. Mater. Chem. A*, 2013, **1**, 3706.

52. H. Cheng, Z. G. Lu, J. Q. Deng, C. Y. Chung, K. Zhang, and Y. Y. Li, *Nano Res.*, 2010, **3**, 895–901.

53. B. Ren, M. Fan, Q. Liu, J. Wang, D. Song, and X. Bai, *Electrochim. Acta*, 2013, **92**, 197–204.

54. F. Meng, Z. Fang, Z. Li, W. Xu, M. Wang, Y. Liu, J. Zhang, W. Wang, D. Zhao, and X. Guo, *J. Mater. Chem. A*, 2013, **1**, 7235.

55. R. R. Bi, X. L. Wu, F. F. Cao, and L. Y. Jiang, Y. G. Guo, and L. J. Wan, *J. Phys. Chem. C*, 2010, 2448–2451.

Table 1: Summary of research on CuO based supercapacitors compared with some key results from other materials such as Co_3O_4, NiO, RuO_2

Morphology	Method of synthesis	C_S (Fg^{-1})	Stability	Discharge current density	Electrolyte	Ref
Nanosheet	Template growth method	569	17.5% loss after 500 cycles	5 $mAcm^{-2}$	6M KOH	15
Nanosheet	Anodization	212	15% loss after 850 cycles	0.41 $mAmg^{-1}$	6M KOH	14
Nanoflower	Simple chemical precipitation	134	5.2% loss after 200 cycles	10 $mAcm^{-2}$	6M KOH	16
Nanoflower	Solution phase	159	5% loss after 850 cycles	0.41 $mAmg^{-1}$	6M KOH	14
Nanoflakes	Oxidation of NaOH	190	33% loss after 2000 cycles	2 $mAcm^{-2}$	1M KOH	12
Lotus-like nanostruct	Liquid solid reaction	278	15% loss after 5000 cycles	2 $mAcm^{-2}$	5M NaOH	17
Cauliflower	Potentio dynamic	162	19% loss after 2000 cycles	2 $mAcm^{-2}$	1M Na_2SO4	13
Nanowire (Dia ~190 nm)	Anodization	102	15% loss after 850 cycles	0.41 $mAmg^{-1}$	6M KOH	14
Co_3O_4 Nanowires	Electrodeposition	768	17% loss after 5000 cycles	5 Ag^{-1}	1M KOH	52
Hollow NiO nanofibers (dia ~120)	Electrospinning	336	13% loss after 1000 cycles	5 $mAcm^{-1}$	6M KOH	53
Porous Co_3O_4 partcles	Solid state conversion process	150	Enhanced at the end of 3400 cycles	1 Ag-1	2M KOH	54
RuO_2 Nanoparticle	Solution based method	648	7% loss after 2000 cycles	Not available	1 M H_2SO_4	55
Nanowire (Dia ~30 nm)	Electrospinning	620	10 % loss after 2000 cycles	5 $mAcm^{-2}$	6M KOH	This work

Figure Captions

Figure 1: The FESEM images of the as-spun PVA/copper acetate composite fibers (top panel) and sintered CuO nanowires (bottom panel) at low (left) and high (right) magnifications.

Figure 2: (a) The bright field TEM images of a typical CuO nanowire and (b) high resolution lattice image of a typical particle composing the wire corresponding to the (111) plane. Inset: SAED image (upper left) and EDX (lower right) pattern.

Figure 3: The XRD pattern of copper oxide nanowires fitted to a monoclinic unit cell. The experimental and simulated intensity data (I_e and I_s) are plotted as circle signs (o) and red solid lines, respectively, and $\Delta I = I_e - I_s$ below. The tick marks indicate the position of all possible Bragg reflections from the CIF file obtained from the Crystallography Open Database collection code COD: 9014580.

Figure 4: The CV data of the CuO nanowire electrode (a) at varying concentration of KOH solution at a scan rate of 10 mV/s; (b) in 3M KOH (c) in 6M KOH aqueous solution and (d) in 3M LiOH at different scan rates between 2 and 70 mVs^{-1}; (e) variation of specific capacitance as a function of scan rate in the two electrolytes. The insets in (b) & (c) show CV at 2 mVs^{-1} showing the oxidation (A1, A2) and reduction (C1, C2) events. Refer the text for assignments of the peaks.

Figure 5: Voltammetric current as a function of (a) scan rate of the CuO electrode in 3M KOH and (b) square root of scan rate in 3M LiOH and 6M KOH electrolytes.

Figure 6: The first three charge – discharge curves of the CuO nanowire electrode (a) in 3M KOH; and (b) in 6M KOH and (c) in 3M LiOH electrolytes at a galvanostatic current density of 2 Ag^{-1} (5 $mAcm^{-2}$). Discharge curves of the CuO nanowire electrode at different current densities (a_1) in 3M KOH; and (b_1) in 6M KOH; and (c_1) 3M LiOH.

Figure 7: Variation of specific capacitance as a function of current density in the KOH and LiOH electrolytes. The filled circle and open squares indicate the experimental data and the solid line is a trend line employing an exponential decay function.

Figure 8: Dependence of the discharge specific capacitance and the Coulombic efficiency as a function of charge –discharge cycle numbers under various conditions. The charge – discharge tests were performed at 5 Ag^{-1} (12.5 $mAcm^{-2}$). The capacitance retention in the respective electrolytes for the 1 – 1000 is in panels (a); the panels (b) shows corresponding variation in the Coulombic efficiency.

Figure 9: Nyquist plot for CuO nanowire electrode at open circuit potentialin KOH and LiOH electrolytes. Inset: a magnified high frequency region of the spectrum showing the electrochemical equivalent resistance (ESR) of the devices.

Figure 10: The variation of the real (*C'*) and imaginary (*C''*) part of the capacitance with the frequency at open circuit potential for (a) 3M KOH electrolyte; and (b) 6M KOH electrolyte, and (c) 3 M LiOH.

Figure 11: Ragone plot showing the specific energy density versus specific power density of the CuO nanowire electrodes.

Vidyadharan et al, Figure 1

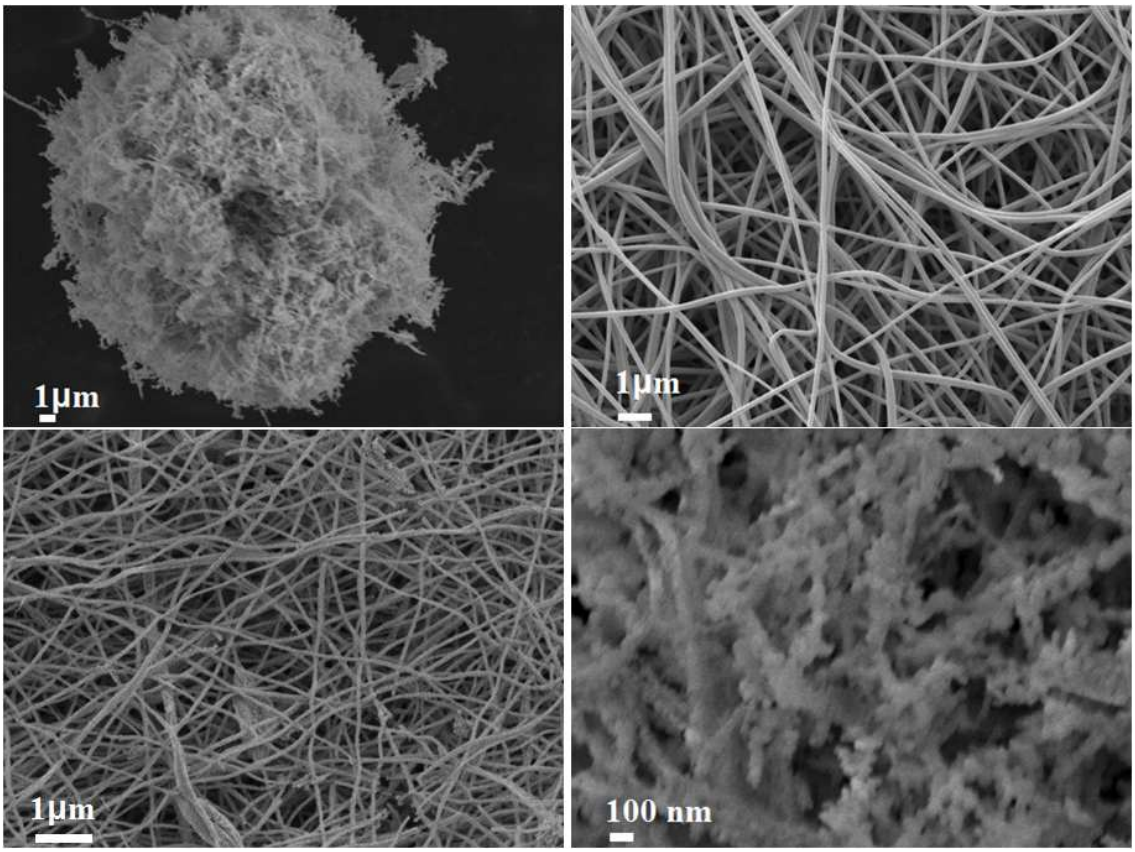

Vidyadharan et al, Figure 2

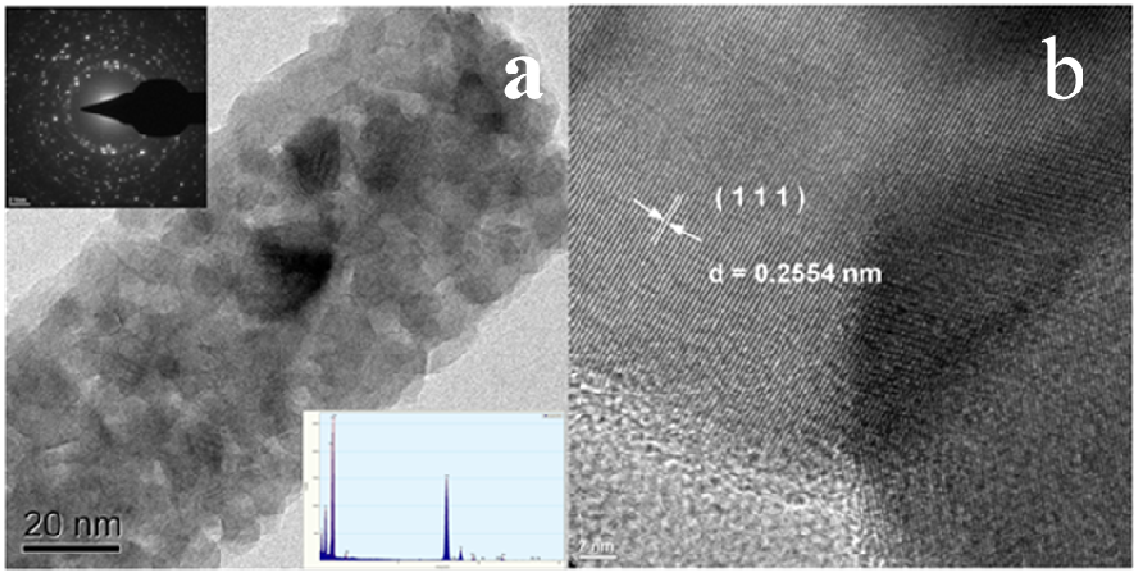

Vidyadharan et al, Figure 3

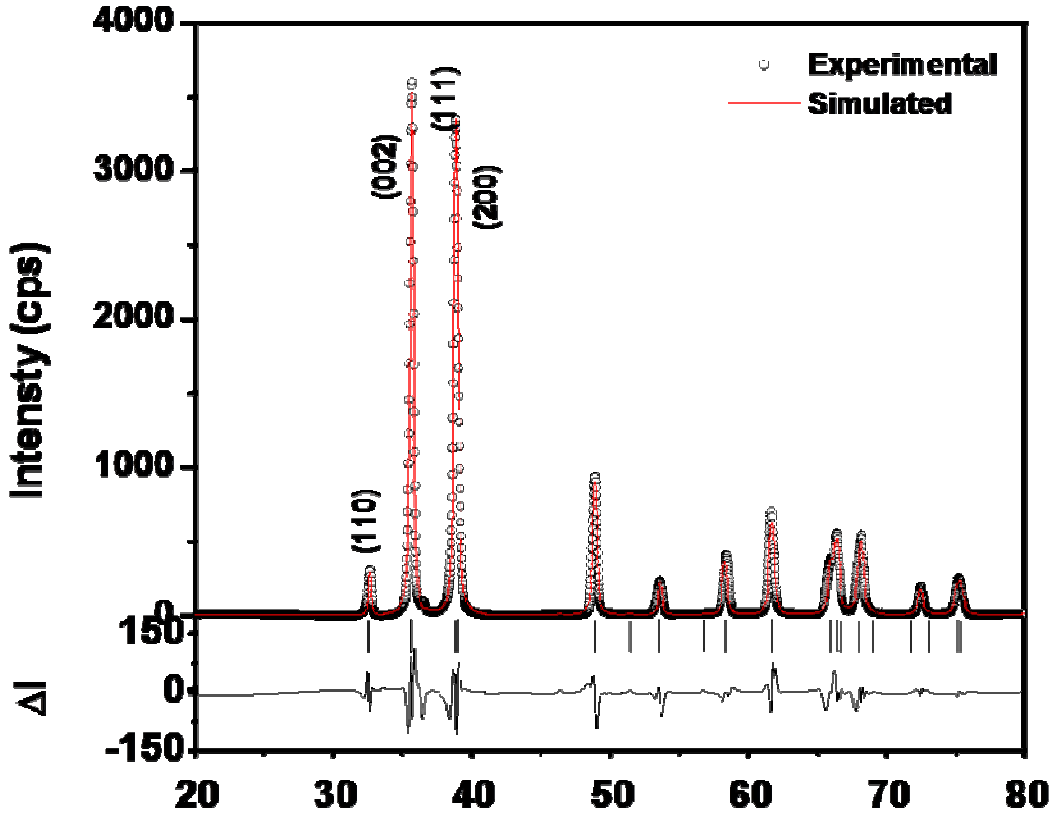

Vidyadharan et al, Figure 4

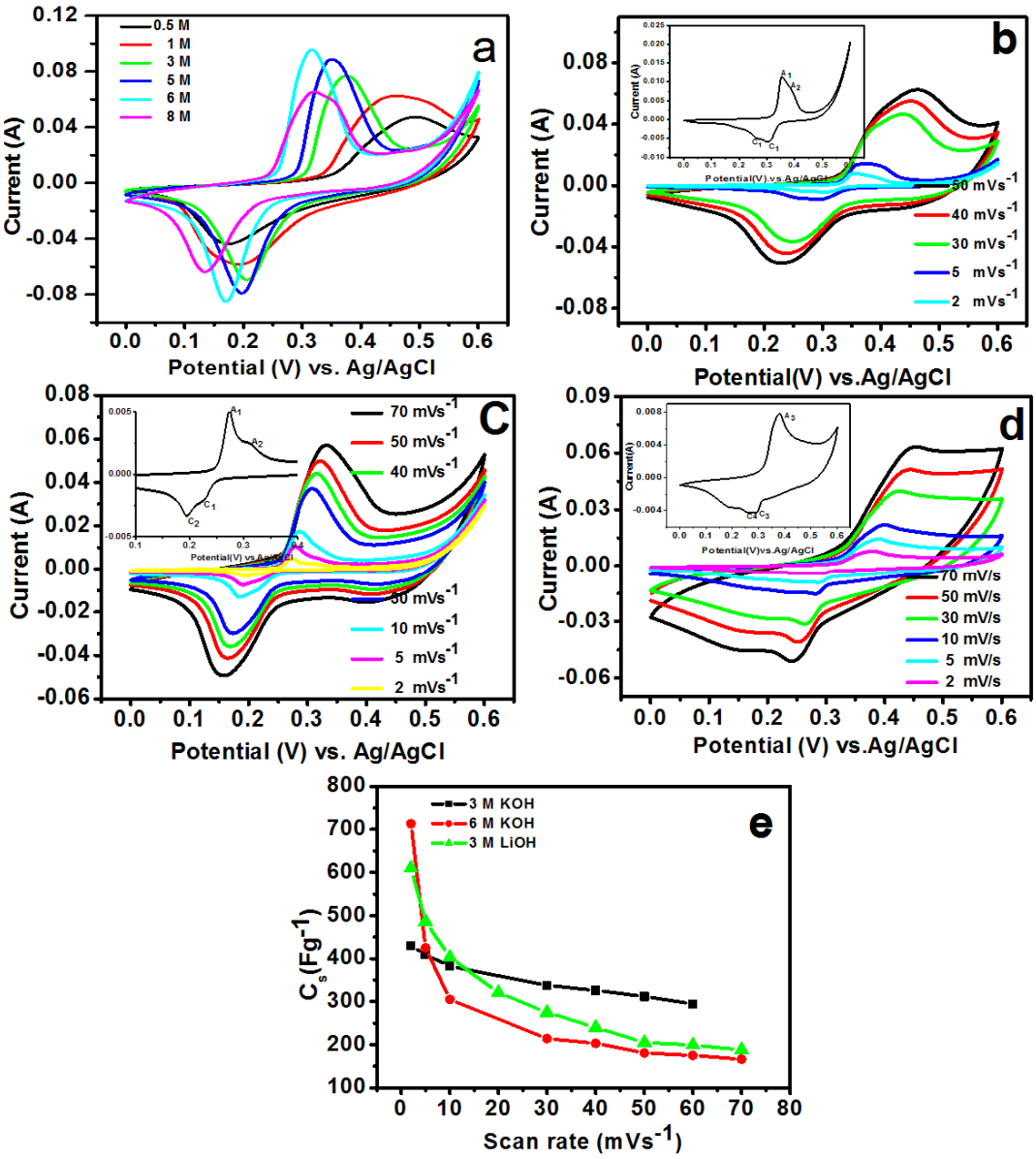

Vidyadharan et al, Figure 5

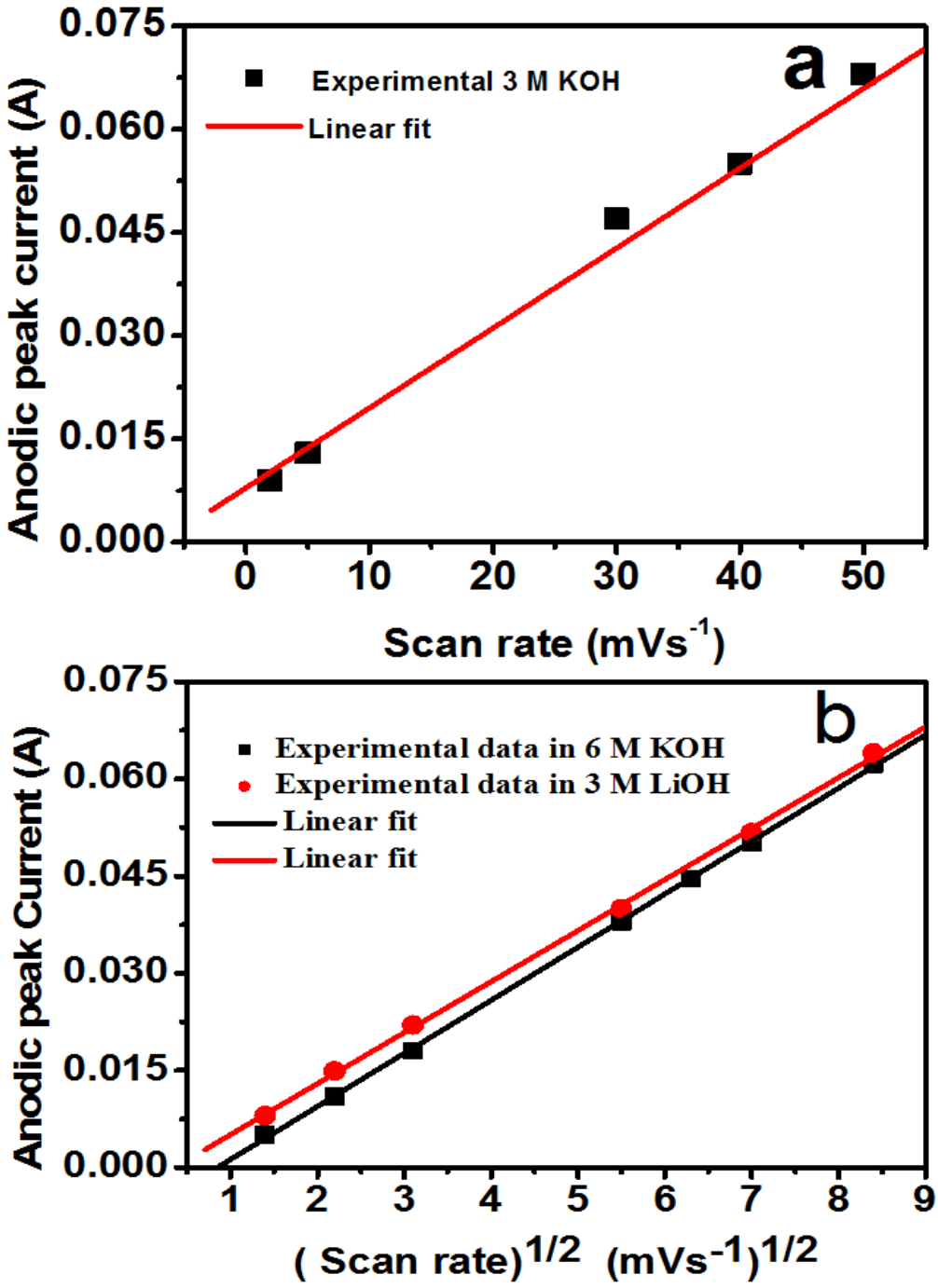

Vidyadharan et al, Figure 6

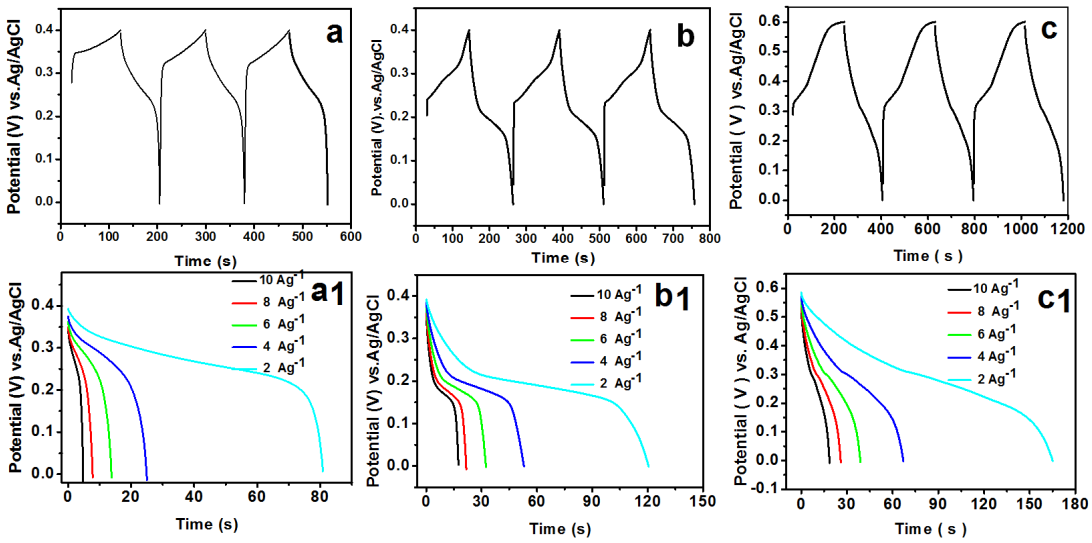

Vidyadharan et al, Figure 7

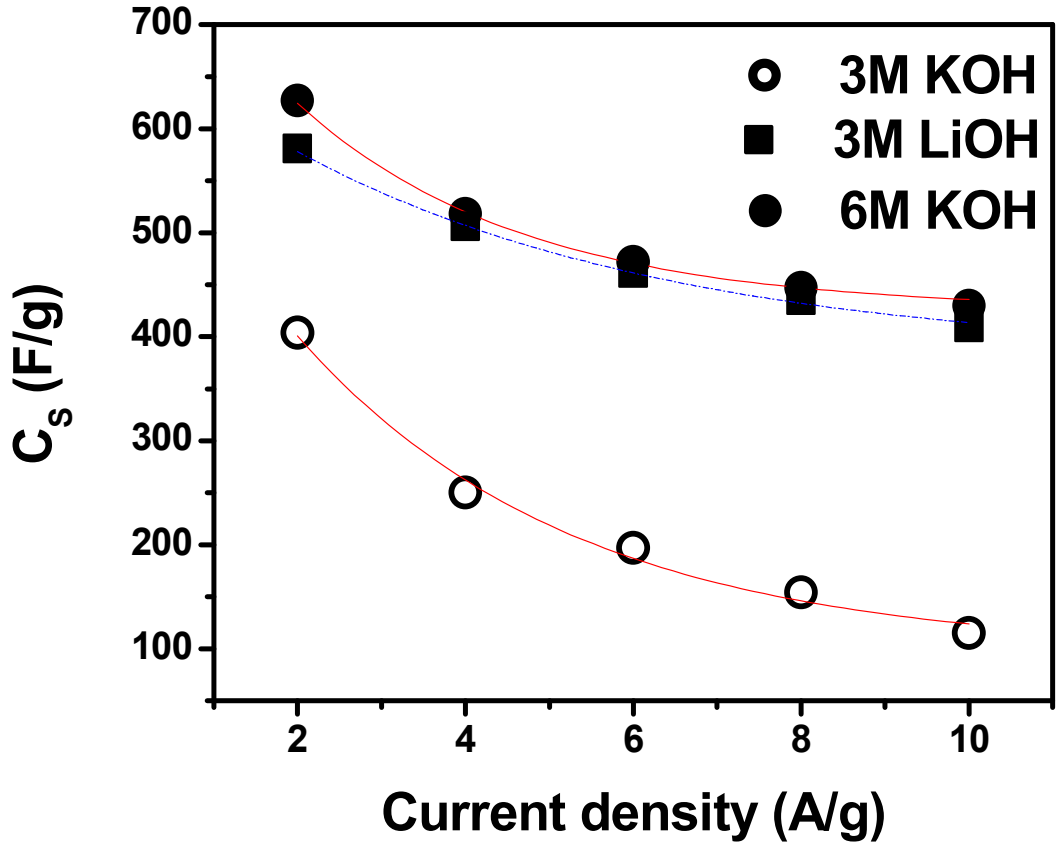

Vidyadharan et al, Figure 8

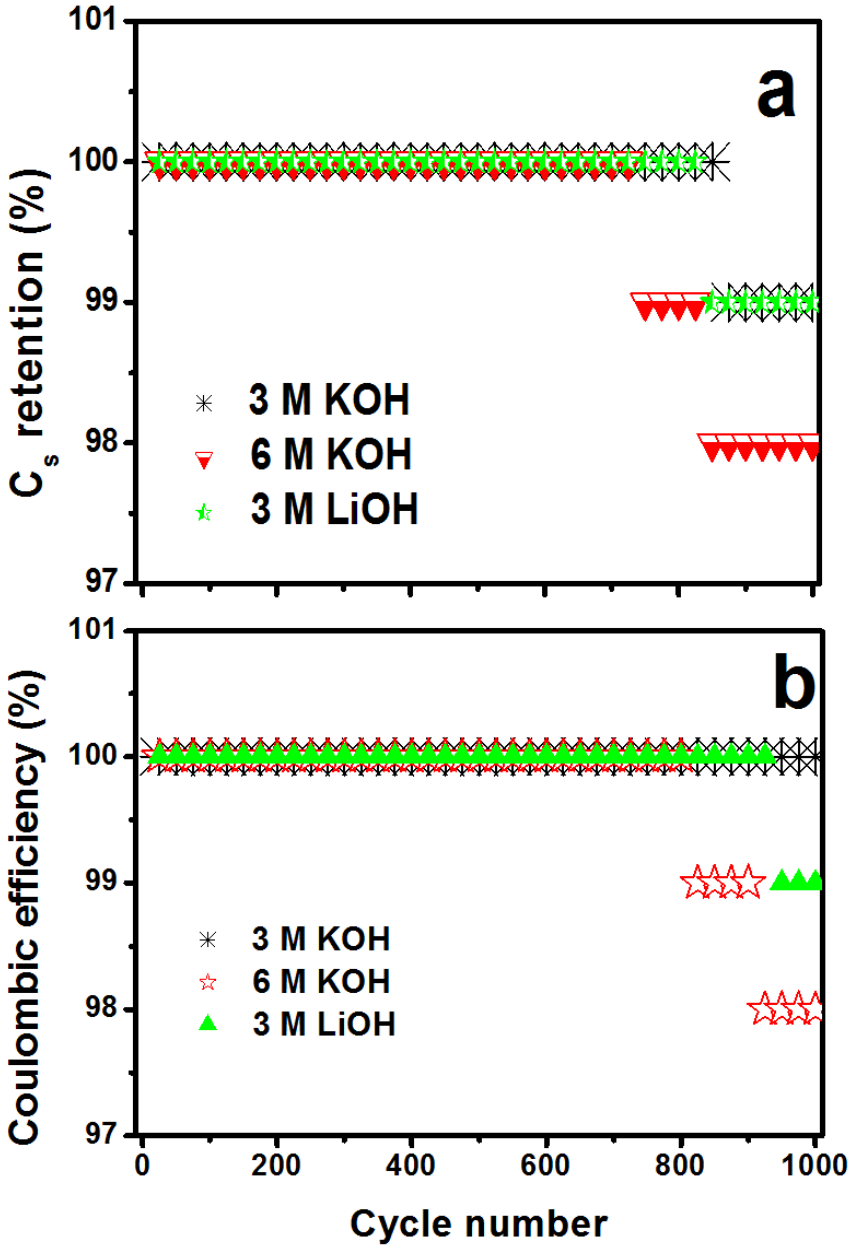

Vidyadharan et al, Figure 9

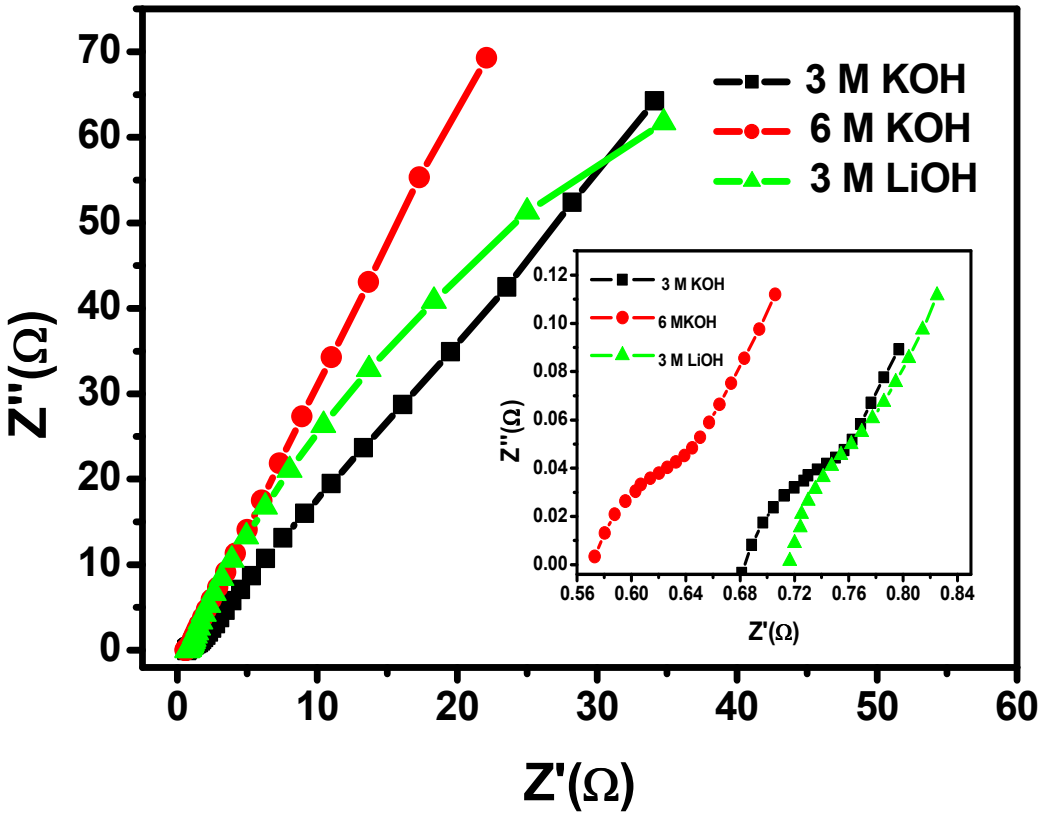

Vidyadharan et al, Figure 10

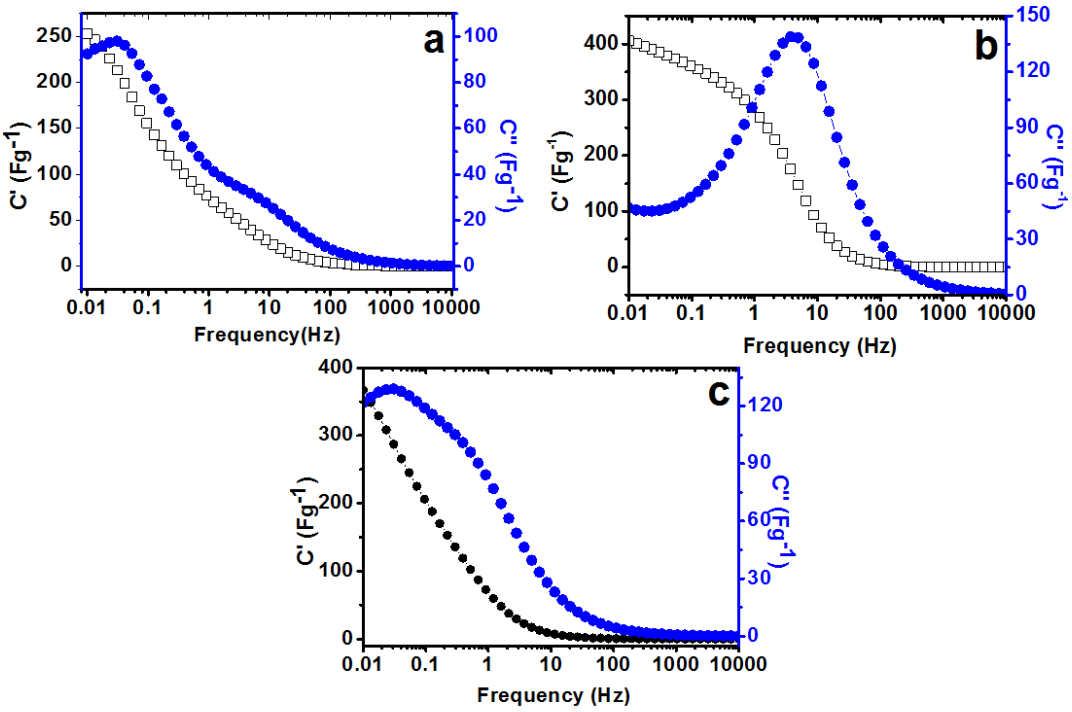

Vidyadharan et al, Figure 11

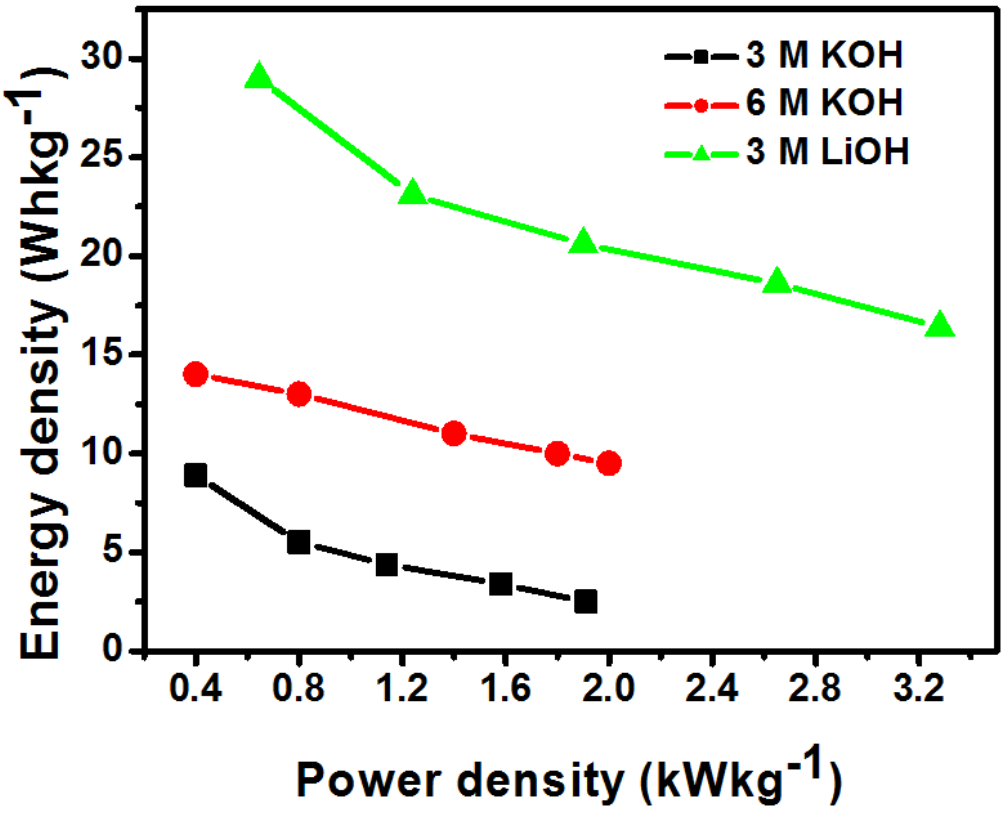

Table of Content Entry

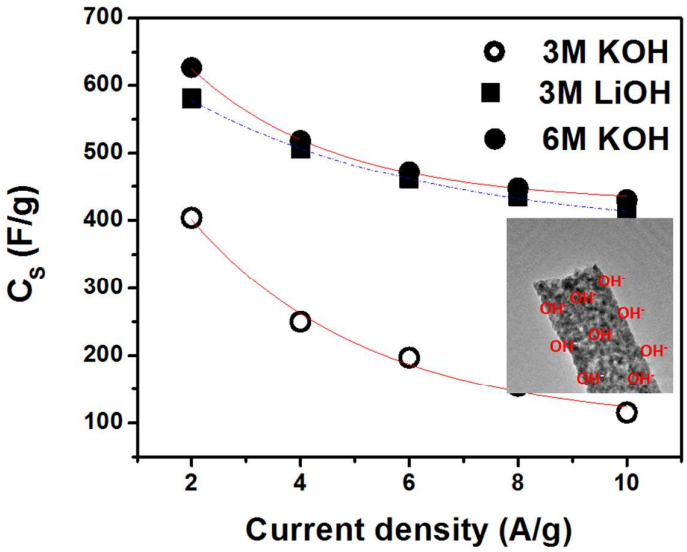

Electrospun CuO nanowires from an aqueous polymeric solution gave the highest specific capacitance so far achieved when tested as a supercapacitor electrode.